Colossal Linear Magnetoelectricity in Polar Magnet Fe$_2$Mo$_3$O$_8$

Yuting Chang,[1,*] Yakui Weng,[2,*] Yunlong Xie,[3,*] Bin You,[1] Junfeng Wang,[1] Liang Li,[1] Jun-Ming Liu[4]
Shuai Dong[5,†] and Chengliang Lu[1,‡]

[1]*Wuhan National High Magnetic Field Center & School of Physics, Huazhong University of Science and Technology, Wuhan 430074, China*
[2]*School of Science, Nanjing University of Posts and Telecommunications, Nanjing 210023, China*
[3]*Institute for Advanced Materials, Hubei Normal University, Huangshi 435001, China*
[4]*Laboratory of Solid State Microstructures, Nanjing University, Nanjing 210093, China*
[5]*Key Laboratory of Quantum Materials and Devices of Ministry of Education, School of Physics, Southeast University, Nanjing 211189, China*

The linear magnetoelectric effect is an attractive phenomenon in condensed matters and provides indispensable technological functionalities. Here a colossal linear magnetoelectric effect with diagonal component α_{33} reaching up to $\sim$480 ps/m is reported in a polar magnet Fe$_2$Mo$_3$O$_8$. This effect can persist in a broad range of magnetic field ($\sim$20 T) and is orders of magnitude larger than reported values in literature. Such an exceptional experimental observation can be well reproduced by a theoretical model affirmatively unveiling the vital contributions from the exchange striction, while the sign difference of magnetocrystalline anisotropy can also be reasonably figured out.

Magnetoelectric (ME) effects refer to the control of magnetization (M) by electric field E or control of polarization (P) by magnetic field H, which provide fascinating functionalities to develop next-generation electronic devices, e.g., ultrasensitive sensors, and energy-saving memories [1–3]. There are various manifestations of ME effects, which can be realized in many kinds of materials including but not limited to ME composites, multiferroics, as well as axion insulators [4]. Of particular interest is the most canonical linear ME effect, i.e., H induces electric polarization $P_i = \alpha_{ij}H_j$, or E causes a variation of magnetization $\mu_0 M_j = \alpha_{ij}E_i$, with α_{ij} the ME tensor and i/j the component of spatial coordinates [5,6]. In those linear magnetoelectrics, the interplay of broken space-inversion and time-reversal symmetries can yield a bunch of emergent physics and functions, including ferrotoroidicity, ME monopole, nonreciprocal transport of quasiparticles, etc. [7–9]. Recently, it was found that the writing threshold could be reduced drastically in a memory device made of the paradigmatic linear ME Cr$_2$O$_3$, implying the technological importance of linear ME in enhancing energy efficiency [10]. Although the studies on linear ME can be traced back to the 1960s, generally the intrinsic linear magnetoelectricity to date remains weak, with typical α values of $1 \sim 10$ ps/m, which has been a long-term issue of ME activities [5,6].

Thermodynamically it is well known that α_{ij} is just bounded by the permittivity ε_{ii} and permeability μ_{jj} of solids, i.e., $\alpha_{ij}^2 < \varepsilon_{ii}\mu_{jj}$ [11]. To obtain large α_{ij}, nonlinear regions of ε_{ii} and μ_{jj} are usually employed, especially near

a critical point of a ME system where the permittivity and/or permeability may be significantly amplified. For example, in those type-II multiferroics where spontaneous P's are generated by some special magnetic orders, magnetic transitions or metamagnetic transitions can trigger remarkable changes of P's and result in very large ME coefficients [12]. However, such a scenario can only work in the proximate region near the transition point. In this sense, the operating window of potential ME devices based on these materials would be narrow.

In fact, the integration upon H is the total change of P (i.e., ΔP). With fixed ΔP, the larger α, the narrower operating H window. Such a trade-off between ME sensitivity and operating window makes it difficult to obtain an optimal system with superior performances in both sides (large α and wide H window), once the total P generated by magnetism is small. Therefore, alternative routes should be developed.

It has been well recognized that the symmetric exchange striction allows much larger P's [e.g., on the order of $\sim$1 μC/cm^2 in E-type antiferromagnetic (AFM) manganites] [13,14], while other mechanisms for magnetism-driven polarization (e.g., the inverse Dzyaloshinskii-Moriya interaction (DMI) and the spin-dependent p-d hybridization) rely on the spin-orbit coupling (SOC) and typically lead to small P's ($\sim$0.001–0.1 μC/cm^2) [15–17]. Nevertheless, only large P's from exchange striction is not sufficient. In fact, some magnetic textures (e.g., E-type phase in o-LuMnO$_3$ [18] and o-YMnO$_3$ [19]) are robust against H, leading to a weak ME response. In other cases,

large nonlinear ME effects, instead of linear ones, occur in a relatively narrow H window, triggered by the first-order phase transitions [20–22]. These facts indicate that additional physical ingredients have to be involved to obtain large linear ME.

In this Letter, the ME response of a polar magnet $Fe_2Mo_3O_8$ is studied. Our experimental study finds a colossal linear ME effect in a broad H window, far beyond the consequence near the first-order transition point. Specifically, the diagonal linear ME component in its ferrimagnetic (FRM) phase is unprecedentedly large: $\alpha_{33} \sim$ 480 ps/m at 20 K, orders of magnitude larger than reported values in literature [5]. Our theoretical calculations suggest that the exchange striction tuned polarity and sign difference of magnetocrystalline anisotropy are essential in physics.

As shown in Fig. 1(a), $Fe_2Mo_3O_8$ consists of Fe-O and Mo-O blocks stacking along the c axis, and the polar arrangement of FeO_4 tetrahedra manifests the crystallographic polarity [23,24]. The corner-shared FeO_4 tetrahedra and FeO_6 octahedra form a buckled honeycomb structure within the ab plane. $Fe_2Mo_3O_8$ has an AFM ground state (magnetic point group $6'mm'$) below $T_N \sim$ 60 K with all Fe^{2+}-spins pointing along the c axis [23], which can be evidenced by the anomalies in the temperature (T) dependence of M as shown in Fig. 1(b). The remarkable difference between $M_c(T)$ and $M_{ab}(T)$ persists up to room temperature, implying its strong magnetic anisotropy. Corresponding to the AFM transition, a sharp peak arises in the T dependence of dielectric constant $\varepsilon(T)$ [Fig. 1(c)], as well as an obvious change of $P_c(T)$ [Fig. 1(d)], revealing the onset of magnetically driven P based on the polar structure. The exchange striction mechanism is responsible for this emergent P [23,24].

By applying $H//c$ axis above a critical field H_{cri}, a FRM phase is stabilized where the Fe tetrahedral and octahedral irons (Fe_T vs Fe_O) form individual ferromagnetic sublattices and align in opposite directions [Fig. 1(a)]. As shown in Fig. 1(e), a jump of $\Delta M_c \sim 0.6$ μ_B/f.u. at H_{cri} indicates that Fe_T and Fe_O sites have different magnetic moments. Concomitantly, the AFM-FRM transition causes striking magnetocurrent at H_{cri}, and the integrated $\Delta P_c(H)$ curve exhibits a steplike anomaly with $\Delta P_c \sim 0.06$ $\mu C/cm^2$, as shown in Figs. 1(f) and 1(g), consistent with the previous report [24]. The H-stabilized FRM phase belongs to the magnetic point group $6m'm'$, which allows diagonal linear ME components. Previous works studied the ME response in a relatively narrow H-T window, and indeed observed approximately linear ME with $\alpha_{33} \sim 16$ ps/m in the FRM phase of $Fe_2Mo_3O_8$, although there were also nonlinear terms mixed in [24,25]. A single-site mechanism, i.e., the g-factor effect, was proposed to explain this linear ME, instead of the symmetric exchange responsible for P, i.e., a two-site mechanism.

In the following, we performed extensive measurements of magnetization and electric polarization over a large H range up to ~58 T using a pulsed high magnetic field apparatus, which allows in-depth exploration of the linear ME of the FRM phase. As shown in Fig. 2(a), $M_c(H)$ measured with $H//c$ axis at $T = 10$ K also displays a clear AFM-FRM transition with a very high critical field $H_{cri} \sim 32$ T, and the related jump remains

FIG. 1. (a) Schematic of crystal and magnetic structures of $Fe_2Mo_3O_8$. (b)–(d) show T dependence of magnetization along the c axis and the ab plane, c-axis dielectric constant ε, and ΔP_c along the c axis, respectively. (e)–(g) H dependences of M_c, magnetocurrent I, and integrated ΔP_c along the c axis at $T = 50$ K, respectively.
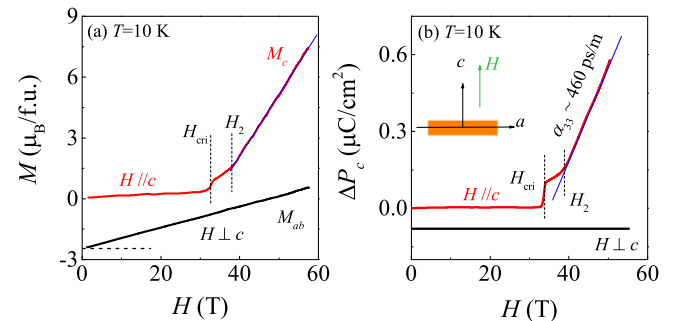
FIG. 2. (a) Out-of-plane (M_c) and in-plane magnetization (M_{ab}) as a function of H measured at $T = 10$ K. (b) H dependence of ΔP_c measured with $H//c$ axis and $H\perp c$ axis at $T = 10$ K. For better view, the black curves are vertically shifted from the zero point.

$\Delta M_c \sim 0.6$ μ_B/f.u. Slightly above H_{cri}, $M_c(H)$ shows another anomaly at $H_2 \sim 39$ T, and then a subsequent linear increase as $H > H_2$. The anomaly at H_2 will be discussed later. M_c reaches ~ 7.5 μ_B/f.u. at $H \sim 58$ T, close to the fully polarized $M \approx 8.5$ μ_B/f.u. for $Fe_2Mo_3O_8$. Different from $M_c(H)$, the in-plane magnetization M_{ab} continuously increases with H, without any anomaly up to $H \sim 58$ T, confirming the strong magnetic anisotropy of $Fe_2Mo_3O_8$.

In accordance with $M_c(H)$, $\Delta P_c(H)$ measured with $H//c$ axis at 10 K also shows an abrupt increase at H_{cri}, and then a crossover anomaly at $H \sim H_2$. A fascinating behavior is the emergence of remarkable and perfect linear enhancement of $\Delta P_c(H)$ above H_2. The estimated linear ME coefficient in a wide range is as large as 460 ps/m, far beyond other known linear ME materials. For instance, $\alpha \sim 4$ ps/m for Cr_2O_3 [26], $\alpha \sim 2$ ps/m for $LiNiPO_4$ [27], $\alpha \sim 10$ ps/m for $GaFeO_3$ [28], $\alpha \sim 30$ ps/m for $TbPO_4$ [29], and $\alpha \sim 40$ ps/m for $Co_4Nb_2O_9$ [30]. With the measured dielectric constant $\varepsilon \sim 15$ at $T < T_N$ for $Fe_2Mo_3O_8$ [Fig. 1(c)], one may translate $dP/dH \sim 460$ ps/m to $dE/dH \sim 2800$ mV/cm-Oe. This value is already comparable with many composite systems, such as commercially used composite $Pb(Zr,Ti)O_3$/terfrnol-D (4800 mV/cm-Oe) [31]. For $H//ab$ plane, $\Delta P_c(H)$ remains zero till the maximum field 58 T, indicating the absence of nondiagonal ME terms.

An interesting phenomenon is that both $\Delta P_c(H)$ and $M_c(H)$ show similar linear behavior above H_2. In particular, $M_c(H)$ exhibits considerable enhancement when $H > H_2$, suggesting drastic modification of the spin arrangement. This is distinctly different from the case of linear magnetoelectrics based on the single-site mechanisms such as the g-factor mechanism and single-ion anisotropy mechanism, which exhibit nearly saturated $M(H)$ behavior as appeared in $(Fe_{1-x}Zn_x)_2Mo_3O_8$ and $Ga_{2-x}Fe_xO_3$ [24,28]. Here the estimated linear $\Delta P_c(H)$ reaches ~ 0.45 $\mu C/cm^2$, which is much larger than the induced P due to the inverse DMI (~ 0.01 $\mu C/cm^2$) [2,15]. Therefore, this remarkable linear variation $\Delta P_c(H)$ is more likely to be due to the exchange striction effect (i.e., two-site mechanism). As mentioned above, a complex ME response was reported at a relatively low H range (i.e., $H_{cri} < H < H_2$) in $Fe_2Mo_3O_8$ [24]. Therefore, the crossover at H_2 could be ascribed to a transition from complex ME response to pure linear ME, namely, from individual magnetic-site effect to two-site mechanism.

Comprehensive characterizations of $M_c(H)$ and ME response have been performed over a broad T range from 1.6 to 50 K. As shown in Fig. 3(a), the AFM-FRM transition is well visible at all measured temperatures, and H_{cri} shifts toward low field with increasing T. H_2 is not as well identified as H_{cri} especially in high-T range (i.e., above 30 K), and just shows slight shift with T, implying different underlying physics. Corresponding behaviors are
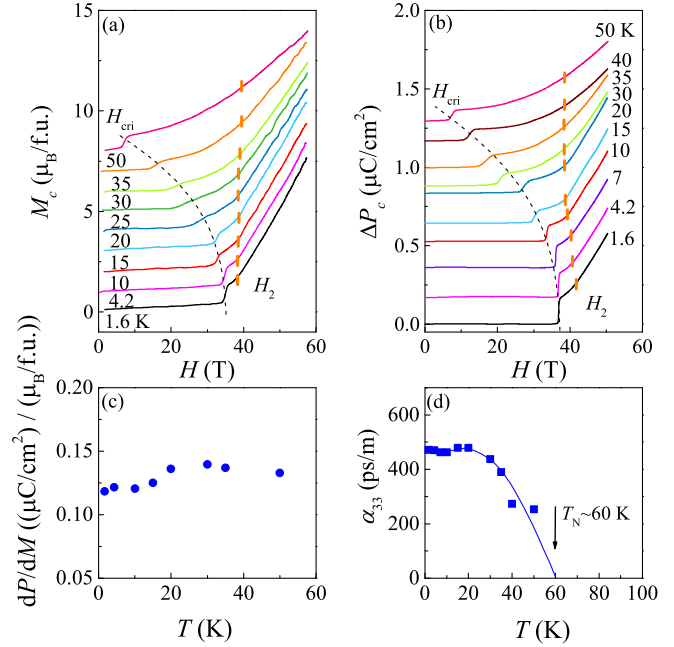
FIG. 3. (a) and (b) show $M_c(H)$ and $\Delta P_c(H)$ at various temperatures, respectively. For a better view, the curves have been shifted vertically. (c) dP/dM as a function of temperature. (d) T dependence of linear magnetoelectricity α_{33}.

also seen in $\Delta P_c(H)$ curves measured at various T's, as shown in Fig. 3(b). Importantly, both $M_c(H)$ and $\Delta P_c(H)$ display almost perfect linear behavior above H_2 at all T's, and the slope shows clear T dependence.

Although here a pulsed magnetic field is used, all the above ME results should be considered as static properties instead of dynamic ones, as confirmed by a comparison study of some key parameters obtained using steady and pulsed magnetic fields (see Supplemental Material, Fig. S3 [32]). The duration time $t \sim 10.5$ ms of the H pulse remains far longer than the timescale of spin dynamics which should be in the THz level for $Fe_2Mo_3O_8$ [33]. Based on the linear behaviors of both $M_c(H)$ and $\Delta P_c(H)$ at high H, it is able to precisely estimate the relationship between M_c and P_c, i.e., dP/dM. As shown in Fig. 3(c), dP/dM distributes roughly at 0.12–0.14 below $T_N \sim 60$ K. The obtained linear ME coefficients α_{33} ($H//c$) are plotted as a function of T in Fig. 3(d), in which α_{33} reaches a plateau of ~ 480 ps/m below 20 K. The colossal linear magnetoelectricity can also be obtained in Zn-substituted $Fe_2Mo_3O_8$ with reduced H_{cri} but robust H_2 (see Supplemental Material [32]).

A previous theoretical work has studied the ME related to phase transitions of $Fe_2Mo_3O_8$ [25]. To understand the colossal linear ME in the FRM phase, we performed density functional theory (DFT) calculations. The AFM ground state and electronic band gap (~ 1.37 eV) can be obtained when a proper U_{eff} and SOC are incorporated simultaneously, in agreement with previous theoretical
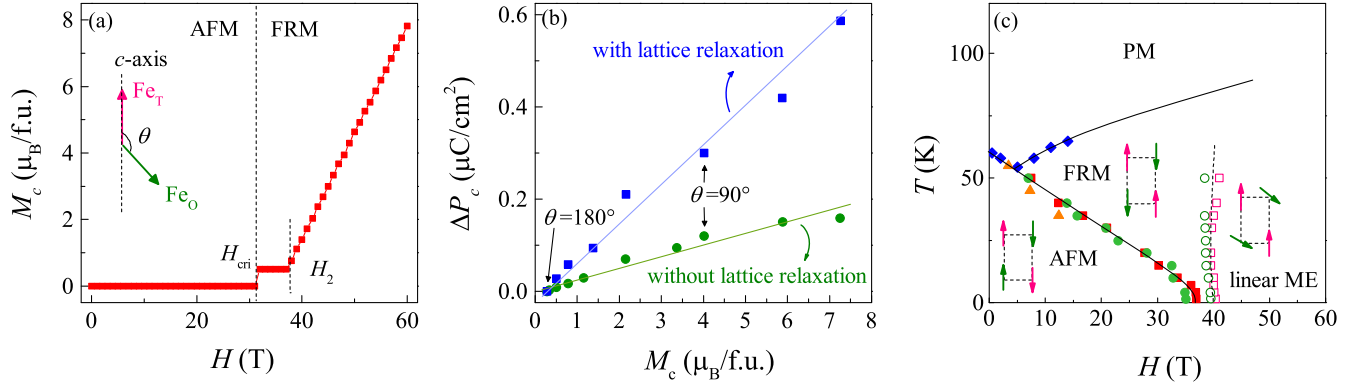
FIG. 4.   (a) The simulated M-H evolution based on the simplified spin model [Eq. (1)]. Model coefficients: $m_O = 4\ \mu_B$, $J_c = -0.46$ meV, $3J_{ab} + J_c = 11.5$ meV, and $A_O = 1.45$ meV. (b) DFT calculated ΔP_c as a function M_c during the spin rotation of m_O. For comparison, both the nonrelaxed case and relaxed one are calculated. In the nonrelaxed case, the crystalline structure is fixed as the optimized FRM phase without spin canting. Thus, only the bias of electron cloud is considered, namely, pure electronic contribution. In the relaxed one, the structure is optimized with SOC enabled to mimic the full contributions from both electronic and lattice. For both cases, the ME behaviors (ΔP_c-M_c) are linear. (c) The ME phase diagram of $Fe_2Mo_3O_8$ constructed based on experimental and theoretical data. Paramagnetic (PM).

works [34,35]. The FRM state is slightly higher in energy (0.14 meV/f.u.) than the AFM one. More details of the DFT calculations can be found in the Supplemental Material [32].

In DFT calculations, the preferred global spin direction is indeed along the c axis, while other orientations lead to higher energy. The local spin moments at Fe_O and Fe_T are -3.74 and $3.68\ \mu_B$, respectively, implying the high-spin states. The orbital moment at the Fe_O site is almost quenched, but the SOC effect yields a significant orbital moment of $0.34\ \mu_B$ for Fe_T, which is parallel to its spin moment. A similar result was also predicted by earlier studies [36,37]. Noting that here the DFT moments, no matter from spin or orbital, are integrated values within the default Wigner-Seitz sphere assigned in pseudopotentials, while the corresponding integrity values of local spin and orbital moments should be 4 and $0.5\ \mu_B$, respectively [36]. Therefore, the large orbital moment of Fe_T is the major contribution to the uncompensated M of FRM phase, leading to the jump $\sim 0.5\ \mu_B$/f.u. in $M_c(H)$ curve at H_{cri} [Fig. 1(e)].

Because of SOC, Fe_T has a much higher magnetocrystalline anisotropy energy (MAE) than Fe_O. According to our DFT study, the easy axis of Fe_T is along the c axis, with a large MAE coefficient $A_T = -5.11$ meV/Fe. However, unexpectedly, the c axis is a hard axis for Fe_O, with a weaker MAE $A_O = 1.97$ meV/Fe. Since A_T is much larger than A_O, the overall MAE prefers the easy axis along the c axis, consistent with the neutron experiments [38]. However, this sign difference of MAE between Fe_T and Fe_O is beyond the previous scenario [23,24], which plays a vital role to determine the ME behavior under field (to be explained below).

Under a magnetic field along the c axis, the magnetic state first transits from the AFM to the FRM phase at H_{cri},

with a net magnetization $\sim 0.5\ \mu_B$/f.u. along the c axis. In other words, the magnetic moment of Fe_T (Fe_O) is parallel (antiparallel) to the magnetic field (i.e., c axis). Further increasing of the magnetic field can only lead to the magnetic canting of Fe_O. Then the free energy during this spin rotation process can be expressed as

$$F = F_0 + [3J_{ab} + J_c] \cdot \cos\theta + A_O \cdot \cos^2\theta - H \cdot m_O \cdot \cos\theta, \tag{1}$$

where J_{ab} (J_c) is the Heisenberg-type effective exchange between in-plane (out-of-plane) nearest-neighboring Fe_O and Fe_T; θ is the moment angle of Fe_O as indicated in the inset of Fig. 4(a). The third item is the MAE of Fe_O; and the last item is the Zeeman energy of Fe_O. Here the MAE and Zeeman energy of Fe_T is not explicitly expressed since they are not changing during the process and thus can be absorbed into the free energy base F_0.

According to Eq. (1), the starting magnetic field to rotate the Fe_O moment is $[3J_{ab} + J_c - 2A_O]/m_O$, corresponding to the experimental H_2. For comparison, H_{cri} at $T = 0$ K to drive the AFM to FMR transition can be expressed as $-2J_c/[m_T$-$m_O]$, which are not identical to H_2 in physics. Based on the experimental value $H_{cri} = 32$ T at 1.6 K and m_T-$m_O = 0.5\ \mu_B$, J_c can be derived as -0.46 meV. And our model based on Eq. (1) (with $3J_{ab} + J_c = 11.5$ meV and $A_O = 1.45$ meV) can well mimic the M-H behavior in the whole range, as shown in Fig. 4(a). First, below H_{cri}, the ground state is AFM, with $M = 0$; Then between H_{cri} and H_2, the magnetic state can be understood as a collinear FMR state without spin canting at $T = 0$ K. Thus the M_c-H curve shows a terrace behavior between H_{cri} and H_2 at low temperature, and thus the ME coefficient in this region is very limited, as revealed in previous studies [24].

After H_2, the magnetic moment of Fe_O starts to rotate, resulting in the increasing of M_c. According to Eq. (1), the M_c-H curve is indeed linear with a slope $m_O^2/2A_O$, reaching ~ 7.5 μ_B/f.u. at 58 T. Note the three independent coefficients $(J_c, 3J_{ab} + J_c, A_O)$ used in our model are very close to the DFT extracted ones (-0.07, 10.55, and 1.97 meV). Considering the simplified spin model and tolerance of DFT values, such a consistent between model and DFT values are rather well, at least in a semiquantitative level. In particular, the sign difference of A_T and A_O is crucial to obtain the linear ME behavior after the terrace. Or if $A_O < 0$, the magnetic transition will be in a sudden jump manner at a critical field (like what occurs at H_{cri}), instead of a continuous rotation of Fe_O spin in a broad region.

The broad-range linear ME behavior suggests that here the spin-related polarization is mainly contributed by the exchange striction, namely, in the form of $\Delta P_c \sim S_{Fe} \cdot S_O \sim \cos\theta \sim \Delta M_c$, instead of the inverse DMI (in the form of $S_{Fe} \times S_O \sim \sin\theta \sim \Delta M_{ab}$). Since exchange striction is a nonrelativistic effect which is relative strong, the ME coefficient here can be so large. Then the concrete value of ΔP_c can be obtained in our DFT calculation by rotating the spin of Fe_O, as shown in Fig. 4(b). Impressively, the ΔP_c-M_c curve due to the Fe_O spin rotation is indeed linear. The DFT estimated slop of $\Delta P_c(M_c)$ is $dP/dM \sim 0.086$ at $T = 0$ K, close to the experimental value of $dP/dM \sim 0.12$ shown in Fig. 3(c).

Based on the above experimental results and theoretical calculations, an (H, T) phase diagram is summarized in Fig. 4(c), where various magnetic phase transitions and crossover behavior of the linear ME are presented. In the low-H region (i.e., below H_{cri}), the AFM state with spins aligned along the c axis is stabilized, and no linear ME is identified. At $H_{cri} < H < H_2$, the AFM phase is transformed to the FRM one, and thus exhibits linear ME. Nevertheless, the linear ME appearing at $H_{cri} < H < H_2$ hosts an individual-site mechanism [24], different from the origin of the magnetically driven P. Above H_2, H is sufficiently large to tune the exchange striction of neighboring Fe^{2+}, leading to another linear ME behavior with colossal coefficient, i.e., $\alpha_{33} = 480$ ps/m at 20 K.

*These authors contributed equally to this work.
†Corresponding author: sdong@seu.edu.cn
‡Corresponding author: cllu@hust.edu.cn

[1] S.-W. Cheong and M. Mostovoy, Nat. Mater. **6**, 13 (2007).
[2] C. L. Lu, M. Wu, L. Lin, and J.-M. Liu, Natl. Sci. Rev. **6**, 653 (2019).
[3] S. Dong, H. Xiang, and E. Dagotto, Natl. Sci. Rev. **6**, 629 (2019).
[4] T. Morimoto, A. Furusaki, and N. Nagaosa, Phys. Rev. B **92**, 085113 (2015).
[5] M. Fiebig, J. Phys. D **38**, R123 (2005).
[6] W. Eerenstein, N. D. Mathur, and J. F. Scott, Nature (London) **442**, 759 (2006).
[7] N. A. Spaldin and R. Ramesh, Nat. Mater. **18**, 203 (2019).
[8] Y. Tokura and N. Nagaosa, Nat. Commun. **9**, 3740 (2018).
[9] S.-W. Cheong, D. Talbayev, V. Kiryukhin, and A. Saxena, npj Quantum Mater. **3**, 19 (2018).
[10] T. Kosub et al., Nat. Commun. **8**, 13985 (2017).
[11] W. F. Brown, R. M. Hornreich, and S. Shtrikman, Phys. Rev. **168**, 574 (1968).
[12] K. Zhai et al., Nat. Commun. **8**, 519 (2017).
[13] S. Picozzi, K. Yamauchi, B. Sanyal, I. A. Sergienko, and E. Dagotto, Phys. Rev. Lett. **99**, 227201 (2007).
[14] I. A. Sergienko, C. Sen, and E. Dagotto, Phys. Rev. Lett. **97**, 227204 (2006).
[15] S. Dong, J.-M. Liu, S.-W. Cheong, and Z. Ren, Adv. Phys. **64**, 519 (2015).
[16] T. Kimura, T. Goto, H. Shintani, K. Ishizaka, T. Arima, and Y. Tokura, Nature (London) **426**, 55 (2003).
[17] H. Murakawa, Y. Onose, S. Miyahara, N. Furukawa, and Y. Tokura, Phys. Rev. Lett. **105**, 137202 (2010).
[18] S. Ishiwata, Y. Kaneko, Y. Tokunaga, Y. Taguchi, T.-h. Arima, and Y. Tokura, Phys. Rev. B **81**, 100411(R) (2010).
[19] S. Ishiwata, Y. Tokunaga, Y. Taguchi, and Y. Tokura, J. Am. Chem. Soc. **133**, 13818 (2011).
[20] N. Lee, Y. J. Choi, M. Ramazanoglu, W. Ratcliff, V. Kiryukhin, and S. W. Cheong, Phys. Rev. B **84**, 020101 (R) (2011).
[21] J. W. Kim et al., Phys. Rev. B **89**, 060404(R) (2014).
[22] L. Ponet, S. Artyukhin, Th. Kain, J. Wettstein, A. Pimenov, A. Shuvaev, X. Wang, S.-W. Cheong, M. Mostovoy, and A. Pimenov, Nature (London) **607**, 81 (2022).
[23] Y. Wang, G. L. Pascut, B. Gao, T. A. Tyson, K. Haule, V. Kiryukhin, and S. W. Cheong, Sci. Rep. **5**, 12268(R) (2015).
[24] T. Kurumaji, S. Ishiwata, and Y. Tokura, Phys. Rev. X **5**, 031034 (2015).
[25] M. Eremin, K. Vasin, and A. Nurmukhametov, Materials **15**, 8229 (2022).
[26] G. T. Rado and V. J. Folen, J Appl. Phys. **33**, 1126 (1962).
[27] T. B. S. Jensen et al., Phys. Rev. B **79**, 092413 (2009).
[28] T. Arima et al., Phys. Rev. B **70**, 064426 (2004).
[29] G. T. Rado, J. M. Ferrari, and W. G. Maisch, Phys. Rev. B **29**, 4041 (1984).
[30] Y. Chang, J. Wang, W. Wang, C. Liu, B. You, M. Liu, S. Zheng, M. Shi, C. Lu, and J.-M. Liu, Phys. Rev. B **107**, 014412 (2023).
[31] A. V. C. J. Ryu, K. Uchino, and H-E. Kim, Jpn. J. Appl. Phys. **40**, 4948 (2001).

[32] See Supplemental Material at http://link.aps.org/supplemental/10.1103/PhysRevLett.131.136701 for more experimental results and theoretical calculations.

[33] T. Kurumaji, Y. Takahashi, J. Fujioka, R. Masuda, H. Shishikura, S. Ishiwata, and Y. Tokura, Phys. Rev. B **95**, 020405 (2017).

[34] K. Park *et al.*, Phys. Rev. B **104**, 195143 (2021).

[35] T. N. Stanislavchuk *et al.*, Phys. Rev. B **102**, 115139 (2020).

[36] S. Reschke, A. A. Tsirlin, N. Khan, L. Prodan, V. Tsurkan, I. Kézsmárki, and J. Deisenhofer, Phys. Rev. B **102**, 094307 (2020).

[37] I. V. Solovyev and S. V. Streltsov, Phys. Rev. Mater. **3**, 114402 (2019).

[38] D. Bertrand and H. Kerner-Czeskleba, J. Phys. (Les Ulis, Fr.) **36**, 379 (1975).